Received: 22 June 2023 | Revised: 19 October 2023 | Accepted: 20 November 2023

DOI: 10.1111/cas.16037

Cancer Science WILEY

ORIGINAL ARTICLE

TGF-β signaling promotes desmoid tumor formation via CSRP2 upregulation

Yu Li[1,2] | Teruaki Fujishita[1] | Emi Mishiro-Sato[1,3] | Yasushi Kojima[1] | Yanqing Niu[1] | Makoto Mark Taketo[4] | Yuya Urano[5] | Tomohisa Sakai[6] | Atsushi Enomoto[5] | Yoshihiro Nishida[7] | Masahiro Aoki[1,8]

[1]Division of Pathophysiology, Aichi Cancer Center Research Institute, Nagoya, Japan

[2]Department of Plastic Reconstructive Surgery, Nagoya University Graduate School of Medicine, Nagoya, Japan

[3]Molecular Structure Center, Institute of Transformative Bio-Molecules (WPI-ITbM), Nagoya University, Nagoya, Japan

[4]Colon Cancer Project, Kyoto University Hospital-iACT, Graduate School of Medicine, Kyoto University, Kyoto, Japan

[5]Department of Pathology, Nagoya University Graduate School of Medicine, Nagoya, Japan

[6]Department of Orthopedic Surgery, Nagoya University Graduate School of Medicine, Nagoya, Japan

[7]Department of Rehabilitation, Nagoya University Hospital, Nagoya, Japan

[8]Department of Cancer Physiology, Nagoya University Graduate School of Medicine, Nagoya, Japan

Correspondence
Teruaki Fujishita and Masahiro Aoki, Division of Pathophysiology, Aichi Cancer Center Research Institute, 1-1 Kanokoden, Chikusa-ku, Nagoya, Aichi 464-8681, Japan.
Email: tfujishita@aichi-cc.jp and msaoki@aichi-cc.jp

Funding information
Japan Society for the Promotion of Science, Grant/Award Number: JP17H01585, JP18H02686 and JP20K07440

Abstract

Desmoid tumors (DTs), also called desmoid-type fibromatoses, are locally aggressive tumors of mesenchymal origin. In the present study, we developed a novel mouse model of DTs by inducing a local mutation in the *Ctnnb1* gene, encoding β-catenin in PDGFRA-positive stromal cells, by subcutaneous injection of 4-hydroxy-tamoxifen. Tumors in this model resembled histologically clinical samples from DT patients and showed strong phosphorylation of nuclear SMAD2. Knockout of SMAD4 in the model significantly suppressed tumor growth. Proteomic analysis revealed that SMAD4 knockout reduced the level of Cysteine-and-Glycine-Rich Protein 2 (CSRP2) in DTs, and treatment of DT-derived cells with a TGF-β receptor inhibitor reduced *CSRP2* RNA levels. Knockdown of CSRP2 in DT cells significantly suppressed their proliferation. These results indicate that the TGF-β/CSRP2 axis is a potential therapeutic target for DTs downstream of TGF-β signaling.

KEYWORDS
desmoid tumors, fibrosis, mouse models, TGF-β, Wnt signaling

Abbreviations: 4HT, 4-hydroxy-tamoxifen; C mice, *Pdgfra-Cre*^{ERT2}/*Ctnnb1*$^{flox(ex3)}$ mice; C.casp3, cleaved caspase 3; CS mice, *Pdgfra-Cre*^{ERT2}/*Ctnnb1*$^{flox(ex3)}$/*Smad4*$^{flox/flox}$ mice; CSRP2, Cysteine-and-Glycine-Rich Protein 2; DTs, desmoid tumors.

Yu Li and Teruaki Fujishita contributed equally to this work.

1 | INTRODUCTION

Desmoid tumors (DTs), also known as desmoid-type fibromatoses, are soft-tissue tumors of mesenchymal origin with intermediate malignancy.[1] DTs are largely sporadic (>90%) and may occur anywhere in the body, but are most frequently found in the abdominal cavity, abdominal wall, and extremities.[2] Up to 80% of sporadic DTs harbor mutations in the *CTNNB1* gene, encoding β-catenin,[3–5] whereas non-sporadic DTs (Gardner's syndrome) are associated with familial adenomatous polyposis (FAP) caused by germline *APC* mutations.[6] Although DTs do not metastasize and have a low mortality risk, they are highly invasive locally and occasionally induce joint contractures and pain, which greatly reduces the activities of daily living and the quality of life of DT patients. As DTs have an extremely high recurrence rate after surgery, non-surgical options such as observation, drug therapy, including non-steroidal anti-inflammatory drugs (NSAIDs) and chemotherapy, and radiotherapy have become treatments of choice.[6] Mutations in *CTNNB1* and *APC* are likely to be driver mutations for DTs; however, Wnt signaling is not easily targetable; thus, identification of novel therapeutic targets is much needed.[7] Here, we present a new mouse model of sporadic DTs that develops fibroblastic tumors with local invasion, after time-specific and site-specific induction of mutant *Ctnnb1* in PDGFRA-positive stromal cells. Using this mouse model, we identified CSRP2 as a potential target of DTs downstream of TGF-β/SMAD4 signaling.

2 | MATERIALS AND METHODS

2.1 | Desmoid mouse model

The creation of *Ctnnb1*$^{flox(ex3)}$ mice has been described previously.[8] *Smad4*$^{flox/flox}$ (*Smad4*$^{tm2.1Cxd}$/J, Stock No. 017462; RRID:IMSR_JAX:017462), *ROSA26-Luciferase* (*Gt(ROSA)26Sor*$^{tm1(Luc)Kael}$/J, Stock No. 005125; RRID:IMSR_JAX:005125), *Trp53*$^{flox/flox}$ (*Trp53*^{tm1Brn}/J, Stock No. 008462; RRID:IMSR_JAX:008462), and B6 Albino (B6N-*Tyr*$^{c-Brd}$/BrdCrCrl, Original Supplier: Charles River Laboratories Japan, Yokohama, Japan) were purchased from Jackson Laboratories (Bar Harbor, ME, USA). *Pdgfra-Cre*^{ERT2} (B6.Cg-Pdgfra<tm1.1(EGFP/cre/ERT2)Hyma>, BRC No. RBRC09616, Riken BioResource Research Center, Tsukuba, Japan) and *ROSA26-GFP* (R26R-H2B-EGFP, CDB0203K, RIKEN Center for Biosystems Dynamics Research, Kobe, Japan) were purchased. These mice were backcrossed at least five times to C57BL/6NJcl (CLEA Japan, Fujinomiya, Japan), and maintained with B6 Albino mice for luminescence measurements. Mice were housed under specific pathogen-free conditions under a 12-h dark/12-h light cycle, and were allowed standard food and water ad libitum.

For tumor induction experiments, equal numbers of 12–14-week-old male and female mice were used in each study. Cre-mediated recombination was induced by topical injection of 0.1 mg of 4-hydroxy-tamoxifen (17308, Cayman Chemical, Ann Arbor, MI, USA) in sunflower oil subcutaneously in femurs or backs for 3 days. Either 15, 40, or 200 days after induction, mice were euthanized. Animal health was observed weekly and, when tumors were detected, three times a week. All animal experiments were carried out according to protocols approved by the Animal Care and Use Committee of Aichi Cancer Center Research Institute.

2.2 | Patients and samples

We recruited retrospectively ($n=20$) patients who were diagnosed with DTs from 2004 to 2022 at Nagoya University Hospital. Medical records were reviewed for clinical features and pathological findings.

All methods and experimental protocols using human tissues were carried out in accordance with relevant guidelines and regulations approved by the Ethics Committee of Nagoya University Graduate School of Medicine (approval numbers 2014-0280-4 and 2017-0127-5).

2.3 | Tumor scoring, histological analysis, and immunostaining

Mice were euthanized and lesions were excised from under the skin. Long and short axial directions of tumors were measured, and lesion volumes were calculated according to the following formula: Tumor volume (mm^3) = length × width × 0.5 (for femoral tumors) or × 2 (for back tumors). After samples were weighed, tumor tissues were fixed overnight in 10% formalin. For histological analysis and immunostaining, paraffin-embedded samples were prepared and tissue sections were sliced at 4 μm. Details of histological analysis and immunostaining are provided in Appendix S1.

2.4 | RNA sequence analysis

Three C and three CS mice were injected in the back with 4-hydroxy-tamoxifen and tumors were harvested 40 days later. After extracting total RNA from tissues with Sepasol-RNA I Super G (09379-84, Nacalai Tesque, Kyoto, Japan), total RNA cleanup and DNA degradation were performed using a FastGene RNA Premium Kit (FG-81250, Nippon Genetics, Tokyo, Japan). Preparation of sequencing libraries from total RNA using an NEBNext Ultra II Directional RNA Kit (E7760, New England Biolabs, Ipswich, MA, USA) and data acquisition using NovaSeq 6000 (Illumina, San Diego, CA, USA) were conducted by Rhelixa (Tokyo, Japan). FASTQ files were preprocessed and quantified by RNA-seq.[9]

2.5 | Proteomic analysis

Desmoid tumor tissues in the backs were collected from three C mice and three CS mice. Proteomic analysis was performed as described previously with slight modifications.[10] Briefly, tissue samples were lysed

with lysis buffer (2M thiourea, 7M urea, 4% CHAPS), purified by methanol–chloroform precipitation, resuspended in 2M urea and 12mM SDC/SLS in 50mM Tris–HCl pH8.5, digested with trypsin and purified. Tandem mass tag (TMT) labeling of peptides, LC–MS analysis, and MS data processing were conducted exactly as described previously.[10]

2.6 | Data analysis, visualization, and enrichment analysis

Data analysis and visualization were performed using R software (R Core Team, 2022). Dot plots, box plots, bar plots, and volcano plots were created using the *ggplot2* package. Principal component analysis (PCA) was performed using the "prcomp" function in R. The "SVM" function in the *e1071* package was used for linear support vector machines (SVMs) with cost and gamma parameters set to default values. We performed enrichment analysis using Metascape.[11] A subset of genes with PC2 loading less than −0.75 in the RNA-seq PCA analysis was used for RNA-seq enrichment analysis. In total, 72 proteins that changed (CS/C) less than 0.8-fold with *p*-values (Welch 2-tailed *t*-test) less than 0.05 were used for proteomic enrichment analysis.

2.7 | Establishment and culture of a mouse DT cell line

A cell line was established from a DT generated in a *Pdgfra-Cre*^{ERT2};*Ctnnb1*$^{flox(ex3)}$/*Trp53*$^{+/flox}$ mouse. Detailed procedures for cell culture and cell proliferation assays are provided in Appendix S1.

2.8 | siRNA treatment

For knockdown experiments, 2×10^5 DT cells were seeded onto six-well plates and transfected with siRNA (20–40nM) using ScreenFect siRNA (295-75003, FUJIFILM Wako). Details of siRNA sequences are provided in Appendix S1.

2.9 | RT-qPCR analysis

Total RNA was purified from DT cells using a FastGene RNA Premium Kit (FG-81250, Nippon Genetics). cDNA was synthesized from 1μg total RNA using FastGene Scriptase II (Nippon Genetics). A qRT-PCR reaction was performed using PowerTrack SYBR Green Master Mix (A46109, Thermo Fisher Scientific, Waltham, MA, USA) and a QuantStudio 3 Real-Time PCR System (A28566, Thermo Fisher Scientific). Rn45s-1 was used as an internal control. Primer sequences were as follows:

CSRP2, 5′-CAAGCCAGAGAGTGCTCAAC-3′ (forward primer), 5′-CAGCATACACGGAATCCCCA-3′ (reverse primer);

Rn45s, 5′-CATGCATCCTCTCTCGGTGG-3′ (forward primer), 5′-CCTCGAGACCGTAAGAAGCC-3′ (reverse primer);

Ctnnb1, 5′-ACGCAGCTGCTGTCCTATTC-3′ (forward primer), 5′-GGCACCAATGTCCAGTCCAA-3′ (reverse primer);

Axin2, 5′-GAAGAGGAGTGGACGTGTGC-3′ (forward primer), 5′-ACATAGCCGGAACCTACGTG-3′ (reverse primer);

Col1a1, 5′-CTGACGCATGGCCAAGAAGA-3′ (forward primer), 5′-CCGTGCCATTGTGGCAGATA-3′ (reverse primer);

Col5a1, 5′-CCTGGTTCAGTGAATTCAAGCG-3′ (forward primer), 5′-TTGTAGGTGACGTTCTGGTGG-3′ (reverse primer);

Vim, 5′-TCCAGAGAGAGGAAGCCGAA-3′ (forward primer), 5′-TTCAAGGTCAAGACGTGCCA-3′ (reverse primer);

Tgfb1, 5′-ACTGGAGTTGTACGGCAGTG-3′ (forward primer), 5′-GGGGCTGATCCCGTTGATT-3′ (reverse primer);

Tgfb2, 5′-TCCCCTCCGAAAATGCCATC-3′ (forward primer), 5′-CAAGCGGAAGACCCTGAACT-3′ (reverse primer);

Tgfb3, 5′-GACTGGCGGAGCACAATGAA-3′ (forward primer), 5′-ACTCTGCCCGGAACAGATTG-3′ (reverse primer).

$N=3$ for all samples, and the expression level of each mRNA relative to the internal control was quantified using the comparative $2^{-\Delta\Delta Ct}$ method.[12]

2.10 | Western blot analysis

Western blot analysis was performed as described previously.[10] Details of reagents and antibodies used are provided in Appendix S1.

2.11 | Quantification and statistical analysis

Sample sizes for experiments were determined based on our previous studies.[10,13] Random assignments and blind assessments were not performed. Statistical analysis was performed in R (https://www.R-project.org/) using the *EZR* package (Saitama Medical Center, Jichi Medical University, Saitama, Japan). Data were analyzed using two-tailed Student's *t*-tests or one-way ANOVA and post hoc Tukey's honestly significant difference (HSD) test. A *p*-value less than 0.05 was considered statistically significant.

3 | RESULTS

3.1 | Induction of β-catenin mutations in PDGFRA-positive stromal cells causes focal formation of DTs

Previous reports have demonstrated that most DT samples from patients express PDGFRA.[14] Therefore, we generated *Pdgfra-Cre*^{ERT2}/*Ctnnb1*$^{flox(ex3)}$ mice on a B6 Albino background (C mice) in which CreERT2 was driven by the *Pdgfra* promoter.[15] Subcutaneous injection of 4HT into the femurs or backs of C mice resulted in the formation of fibroblastic tumors at the sites of injection (Figure 1A,B). 4HT injection into the backs produced larger tumors than injection into femurs (Figure S1A). Fibroblastic tumors that developed in C

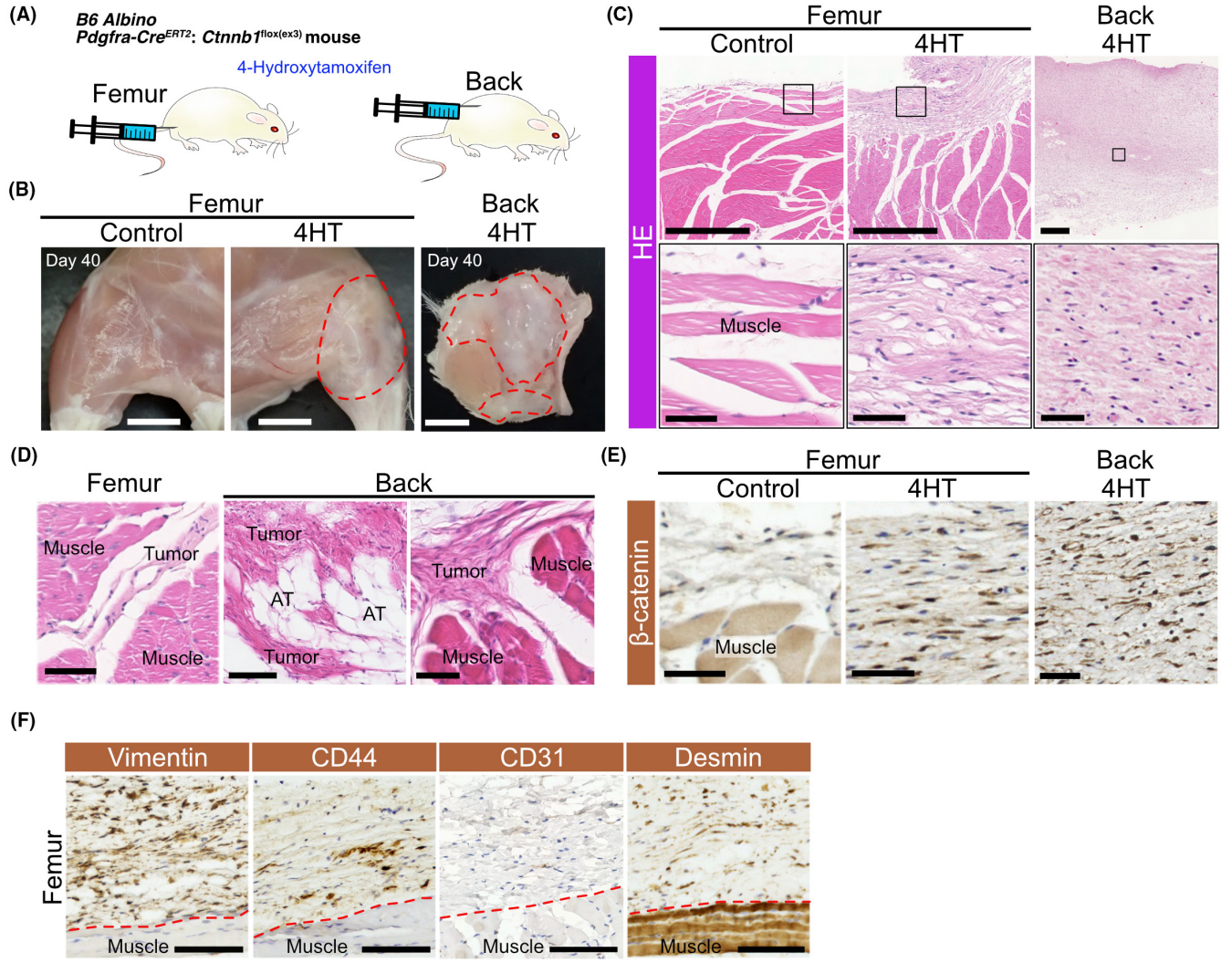

FIGURE 1 A stabilizing mutation of β-catenin in PDGFRA-positive stromal cells causes focal fibroblastic lesions in mice. (A) Schematic representation of induction of fibroblastic tumors by local subcutaneous administration of 4-hydroxy-tamoxifen (4HT) in *Pdgfra-Cre*$^{ER^{T2}}$;*Ctnnb1*$^{+/flox(ex3)}$ mice (C mice). (B) Representative photographs of fibroblastic lesions in the femurs and backs of C mice 40 days after 4HT injection. (Left) Non-injected femur of a C mouse. (Center) fibroblastic lesions developed in the injected femur of a C mouse. (Right) Fibroblastic lesions in the dorsal subcutaneous region. Scale bars: 5 mm. Red dashed lines indicate tumor regions. AT, adipose tissue. (C) Representative images for H&E staining of fibroblastic tumors in C mice. Scale bars: 500 μm for top panels and 50 μm for bottom panels. (Left panels) Femoral muscle and surrounding tissues of control mice. Muscle: femoral muscle. (Center) A fibroblastic tumor around the femoral muscle. (Right) A fibroblastic tumor in the dorsal subcutaneous region. (D) Representative images for H&E staining of tumor cells invading surrounding muscle and adipose tissues. Scale bars: 50 μm. Image of the femur (left) is from the upper center panel in (C). (E) Immunostaining of β-catenin in fibroblastic tumors of C mice. Scale bars: 50 μm. The order of panels is the same as in (C). (F) Immunostaining of vimentin, CD44, CD31, and desmin in fibroblastic tumors developed around the femoral muscle of C mice. Scale bars: 100 μm. Red dashed lines indicated the border between the tumor and the muscle layer.

mice showed histological resemblance to DTs in patients, exhibiting long fascicular arrangements of spindle cells infiltrating surrounding muscle and adipose tissues (Figure 1C,D). Immunohistochemical analysis showed that tumors from C mice strongly expressed DT markers such as β-catenin, desmin, vimentin, and CD44, but not CD31, a negative marker for DTs (Figure 1E,F).[16,17] To determine the time course of tumor growth in C mice, we next generated compound mutant C mice with ROSA26-LSL-Luc mice for in vivo imaging. We found that the luminescence intensity of tumors in the back increased for 20 days after 4HT injection, but then plateaued for the next 60 days. Although tumors in some mice gradually decreased in size, they did not regress completely and remained in the body for ~200 days (Figure S1B–D). Histological and immunohistochemical analyses showed that, on day 15, lesions contained more Ki67-positive, proliferating fibroblastic cells than those on day 40; whereas few apoptotic cells were observed in lesions on days 15 and 40 (Figure 2A). When C mice crossed with ROSA26-LSL-H2B-EGFP mice were injected dorsally with 4HT (Figure S2A), on day 15, tumors contained more fibroblastic cells expressing Sca1 or Thy1, markers of mesenchymal stem cells, while those on day

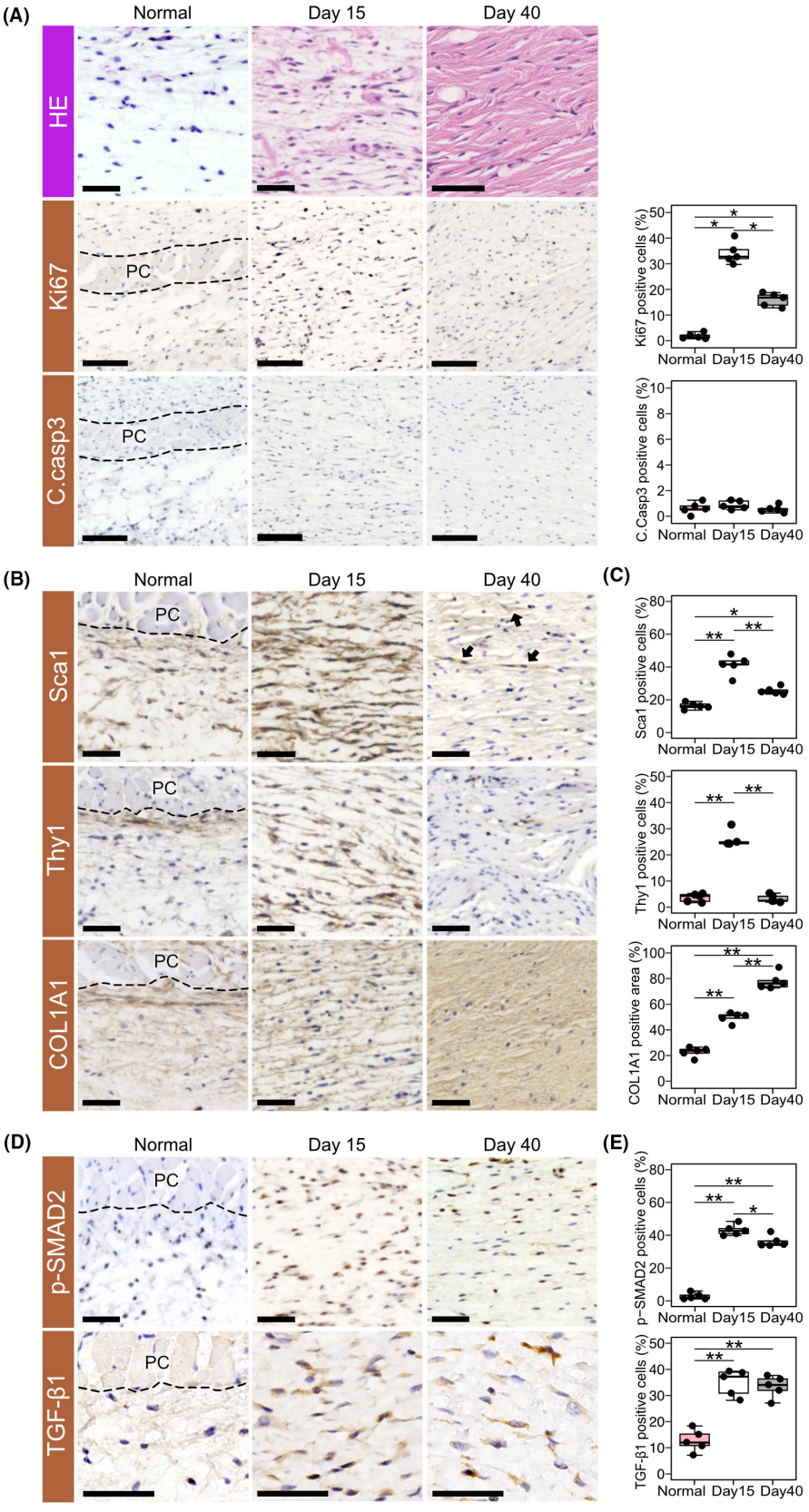

FIGURE 2 Differentiation status of desmoid tumors differs between the early and late stages of development. (A) Images for H&E staining (top) and immunostaining for Ki67 (middle), and C.casp3 (bottom) in representative tumors from the backs of C mice at days 15 and 40. Scale bars: 50 μm for H&E staining and 100 μm for other panels. PC: panniculus carnosus. Normal: Normal subcutaneous tissue of tumor margins at day 40. (Right) Percentages of Ki67-positive and C.casp3-positive cells in fibroblastic tumors in the backs of C mice ($n = 5$). Data are presented as dot plots and box plots. Statistical significance was assessed using one-way ANOVA and Tukey's HSD test. $^{*}p < 0.01$. (B) Immunostaining of Sca1 (top), Thy1 (middle), and COL1A1 (bottom) in representative fibroblastic tumors in the backs of C mice at days 15 and 40. Scale bars: 50 μm. Normal: Normal subcutaneous tissue of tumor margins at day 40. Arrows indicate Sca1-positive cells at day 40. (C) Quantification of percentages of Sca1-positive (top) and Thy1-positive cells (middle) and the percentage of COL1A1-positive area (bottom) in fibroblastic tumors in the backs of C mice ($n = 5$). (D) Immunostaining of phospho-SMAD2 (top) and TGF-β1 (bottom) in fibroblastic tumors in the backs of C mice. Normal: Normal subcutaneous tissue of tumor margins at day 40. Scale bars: 50 μm. (E) Quantification of percentages of phospho-SMAD2-positive cells (top) and TGF-β1-positive cells (bottom) in fibroblastic tumors in the backs of C mice ($n = 5$). Data are presented as dot plots and box plots (C, E). Statistical significance was assessed with one-way ANOVA and Tukey's HSD test. $^{*}p < 0.01$, $^{**}p < 0.001$.

40 contained more eosinophilic cytoplasm and collagenous matrix (Figure 2B,C). Fibroblastic tumor cells, including Sca1-positive or Thy1-positive cells, expressed nuclear GFP (Figure S2B,C), indicating that DTs in C mice were indeed derived from Cre-mediated recombination in PDGFRA-positive cells. These results suggested that desmoid tumors in C mice may have two phases: a highly proliferative phase enriched in stem-like cells and a more stable phase with highly differentiated DT cells.

3.2 | TGF-β signaling promotes DT formation in mouse models

As TGF-β is a universal driver of fibrosis and has been implicated in the growth of DTs,[18–20] we next performed immunohistochemistry for p-Smad2 and TGF-β1 in DTs of C mice. The frequency of p-Smad2-positive cells in DTs on day 15 was elevated compared with normal tissues and slightly decreased on day 40. TGF-β1-expressing cells were observed in DTs on both days 15 and 40, suggesting autocrine activation of the TGF-β pathway in DT cells of C mice (Figure 2D,E).

The TGF-β signaling pathway encompasses multiple ligands (Tgf-β1, Tgf-β2, Tgf-β3), R-Smads (Smad2, Smad3), and a single Co-Smad (Smad4). To address the possible function of TGF-β signaling in DT formation in C mice, we then introduced SMAD4 knockout by crossing C mice with *Smad4*$^{flox/folx}$ mice to generate *Pdgfra-Cre*^{ERT2}; *Ctnnb1*$^{flox(ex3)}$/*Smad4*$^{flox/folx}$ mice, (CS mice) (Figure 3A). Fibroblastic tumors in CS mice, 40 days after 4-HT injection, were significantly

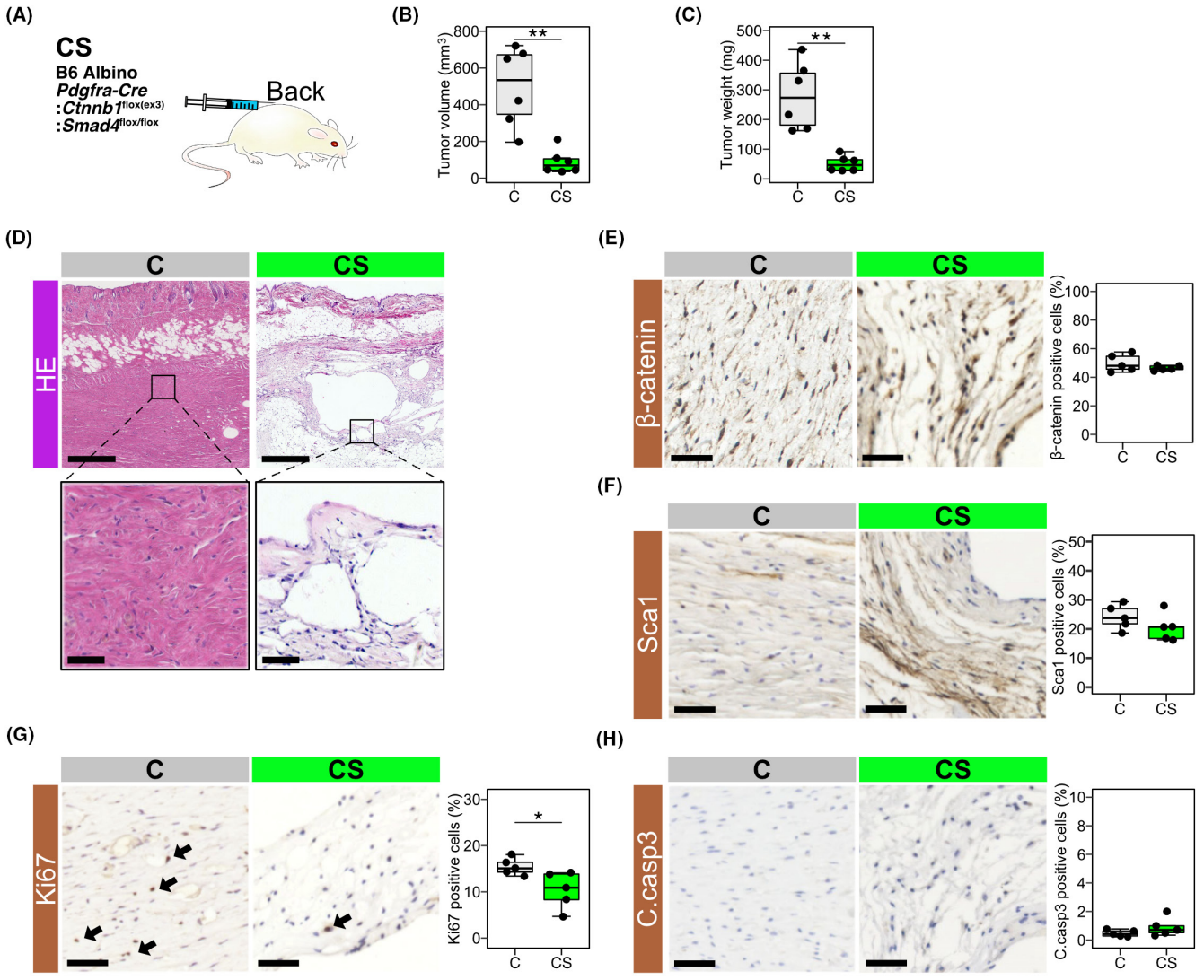

FIGURE 3 Activation of TGF-β/SMAD4 signaling is required for desmoid tumor formation. (A) Induction of fibroblastic tumors by local administration (back) of 4HT in *Pdgfra-Cre*^{ERT2};*Ctnnb1*$^{+/flox(ex3)}$/*Smad4*$^{flox/flox}$ mice (CS mice). (B) Effect of SMAD4 knockout on fibroblastic tumor formation in C mice. Volumes of tumors in the backs of C and CS mice and measured at day 40 after 4HT injection. (C) Weights of tumors in the backs of C and CS mice at day 40. (D) Images for H&E staining of fibroblastic tumors in C (left) and CS (right) mice. Scale bars: 500 μm for top panels and 50 μm for bottom panels showing enlarged views of the frames in the top panels. (E) Immunostaining of β-catenin in fibroblastic tumors in C and CS mice. Scale bars: 50 μm. (Right) Percentages of β-catenin-positive cells in tumors in the backs of C and CS mice ($n = 5$). (F) Immunostaining of Sca1 in fibroblastic tumors in C and CS mice. Scale bars: 50 μm. (Right) Quantification of the percentage of Sca1-positive cells in tumors in the backs of C and CS mice ($n = 5$). (G) Immunostaining of Ki67 in fibroblastic tumors in C and CS mice. Scale bars: 50 μm. (Right) Quantification of the percentage of Ki67-positive cells in tumors in the backs of C and CS mice ($n = 5$). Arrows indicate Ki67-positive cells. (H) Immunostaining of cleaved caspase 3 (C.casp3) in fibroblastic tumors in C and CS mice. Scale bars: 50 μm. (Right) Quantification of the percentage of C.casp3-positive cells in tumors in the backs of C and CS mice ($n = 5$). Data are presented as dot plot and box plots (B, C, and E–H). Statistical significance was assessed with a two-tailed Student's *t*-test. $^{*}p < 0.05$, $^{**}p < 0.01$.

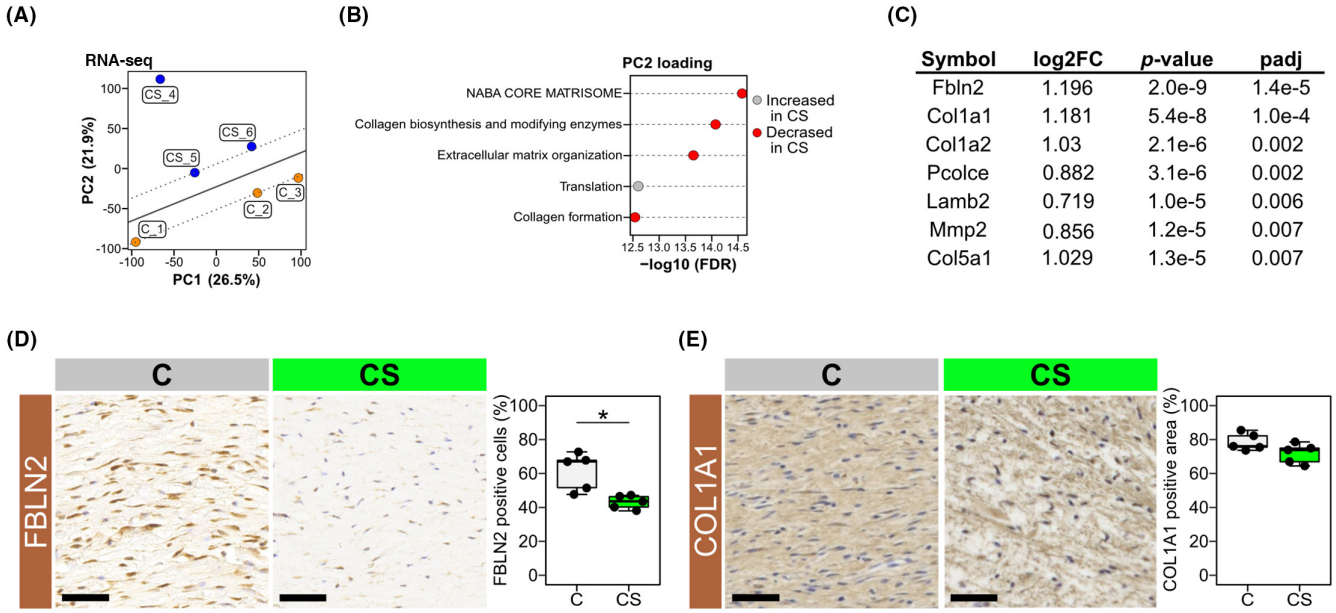

FIGURE 4 SMAD4 knockout decreases the expression of ECM genes in desmoid tumors. (A) PCA analysis of RNA-seq data from desmoid tumors in the backs of *Pdgfra-Cre*^{ERT2};*Ctnnb1*$^{+/flox(ex3)}$ mice (C mice) and *Pdgfra-Cre*^{ERT2};*Ctnnb1*$^{+/flox(ex3)}$/ *Smad4*$^{flox//flox}$ (CS mice). (B) Enrichment analysis of PC2 loadings from PCA analysis in (A) using Metascape. Gray and red circles indicate gene sets for which expression was increased or decreased, respectively, in CS tumors compared with C tumors. (C) List of ECM-related genes significantly more highly expressed in C tumors compared with CS tumors using RNA-seq analysis. (D) Immunostaining of FBLN2 in desmoid tumors of C and CS mice. Scale bars: 50 μm. (Right) Quantification of the percentage of FBLN2-positive cells in tumors in the backs of C and CS mice ($n = 5$). (E) Immunostaining of COL1A1 in desmoid tumors of C and CS mice. Scale bars: 50 μm. (Right) Percentages of COL1A1-positive cells in tumors in the backs of C and CS mice ($n = 5$). Data are presented as dot and box plots (D, E). Statistical significance was assessed with a two-tailed Student's *t*-test. $^{*}p < 0.01$.

smaller in size and mass than those in C mice (Figure 3B,C). Histological analysis showed that tumors in CS mice contained numerous cysts (Figure 3D). As there was no significant difference in the number of β-catenin-positive or Sca1-positive cells between C and CS tumors, TGF-β may have little effect on β-catenin levels or stem-like properties of DT cells (Figure 3E,F). Although apoptotic cells were rarely found in C or CS tumors, Ki67-positive proliferating cells in tumors were decreased in CS mice compared with C mice (Figure 3G,H). These results indicated that the activation of TGF-β/SMAD4 signaling is essential for the growth of DTs in C mice.

To better understand TGF-β/SMAD4 signaling in the proliferation of DT cells at the gene expression level, we performed RNA-seq analysis and proteome analysis for tumors from C and CS mice. PCA analysis of RNA-seq data showed that C tumors and CS tumors could be separated across the PC2 axis (Figure 4A). UniProt annotation score analysis on PC2 loading indicated decreased ECM-related genes, such as those encoding FBLN2, COL1A1, COL1A2, and PCOLCE, in DTs from CS mice, compared with those from C mice (Figure 4B,C). IHC analysis observed that COL1A1 tended to decrease in CS with no significant difference, while FBLN2 decreased significantly (Figure 4D,E). Conversely, enrichment analysis of proteome data showed decreased mitochondria-related and fibroblast-related proteins in CS tumors compared with C tumors (Figure 5A). We then focused on CSRP2, one of the most downregulated proteins in CS tumors, based on proteomic data (Figure 5B). CSRP2 is expressed mainly in vascular smooth muscle cells (VSMCs) and inhibits their migration.[21] We validated the expression of CSRP2 in DTs in our models by immunostaining and found that the frequency of tumor cells expressing CSRP2 was reduced in CS tumors compared with C tumors (Figure 5C,D). Immunostaining of surgically resected samples from DT patients revealed CSRP2-positive and phospho-SMAD2-positive cells in 19 of 20 cases, regardless of their sites of origin (Figure 5E; Figure S3, Table S1). These results suggested that CSRP2 was expressed in DT cells in both mouse models and human patients, and that it may be related to TGF-β/SMAD4 signaling.

3.3 | CSRP2 promotes DT cell proliferation downstream of the TGF-β/SMAD4 signaling pathway

To explore a possible relationship between the TGF-β/SMAD4 pathway and CSRP2, we attempted to establish cell lines derived from DTs in C mice. Primary fibroblasts isolated from DTs in C mice could not be passaged long enough to obtain the number of cells needed for analysis. To circumvent this problem, we generated *Pdgfra-Cre*^{ERT2};*Ctnnb1*$^{flox(ex3)}$/*Trp53*$^{+/flox}$ mice (CP mice) and found that 4HT injection induced the formation of DTs that histologically resemble those in C mice (Figure S4A). We were then able to establish a cell line (DT cells) from CP desmoid tumors.

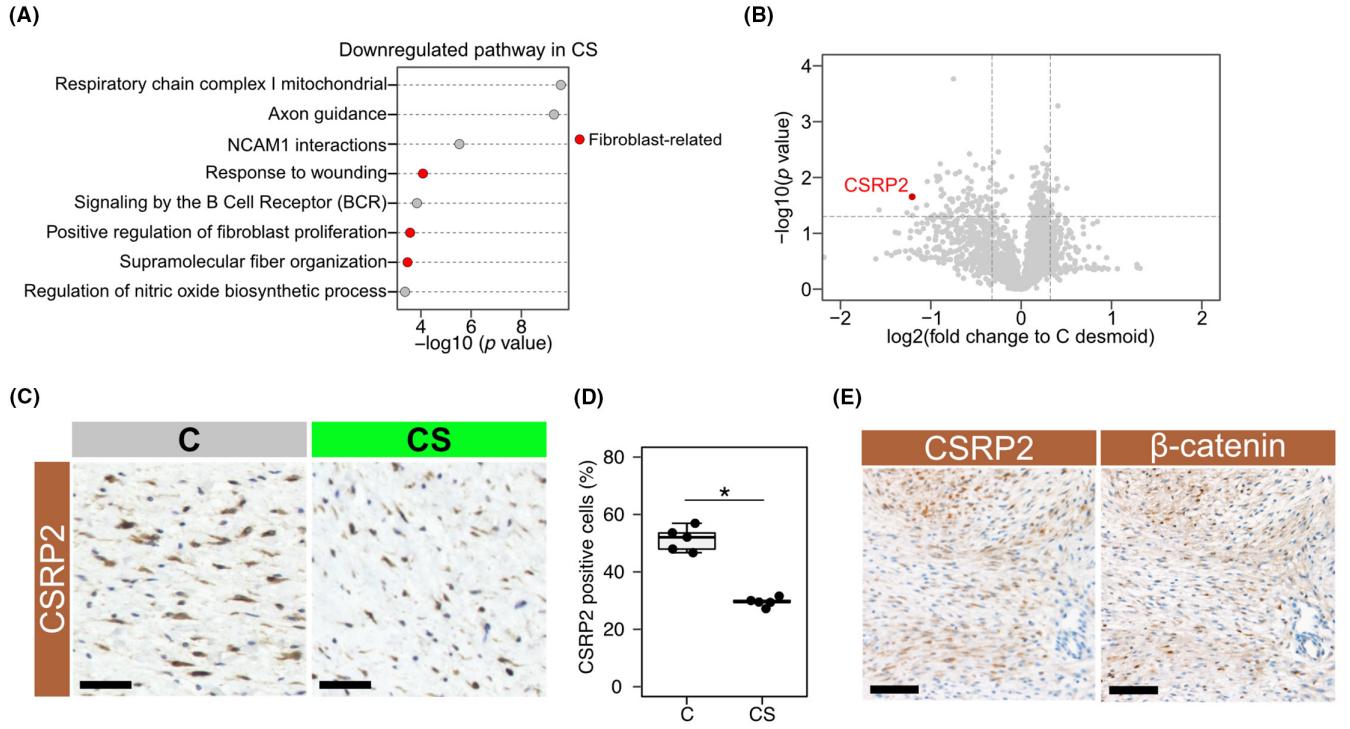

FIGURE 5 SMAD4 knockout decreases the CSRP2 level in desmoid tumors. (A) Enrichment analysis of proteomic data from desmoid tumors in the backs of C and CS mice. Red circles indicate fibroblast-related pathways. (B) Volcano plot of proteomic data from desmoid tumors in the backs of C and CS mice. *p*-values were calculated using Welch's two-tailed *t*-test. CSRP2: cysteine-and-glycine-rich protein 2. (C) Immunostaining of CSRP2 in desmoid tumors of C and CS mice. Scale bars: 50 μm. (D) Quantification of percentages of CSRP2-positive cells in tumors in back lesions of C and CS mice ($n = 5$). Data are presented as dot and box plots. Statistical significance was assessed using a two-tailed Student's *t*-test. $^{*}p < 0.001$. (E) Representative images of immunostaining for CSRP2 (left) and β-catenin (right) in tumor sections from a desmoid tumor patient. Scale bars: 100 μm.

To address the role of TGF-β signaling in the proliferation of DT cells in vitro, we treated them with the TGF-β receptor inhibitor, SB431542. SB431542 significantly suppressed the proliferation of DT cells in a dose-dependent manner, accompanied by reduced phosphorylation of SMAD2 (Figure 6A,B). To determine whether the TGF-β/SMAD4 pathway was involved in regulating CSPR2 expression in DTs, we examined the effect of SB431542 on CSRP2 levels in DT cells. qRT-PCR analysis and western blot analysis showed that SB431542 treatment reduced CSRP2 expression at the mRNA and protein levels, indicating that the TGF-β/SMAD4 pathway positively regulated CSRP2 expression in DT cells (Figure 6C,D). We next investigated the effect of CSRP2 knockdown on the proliferation of DT cells. Two siRNAs targeting CSRP2 significantly suppressed the proliferation of DT cells (Figure 6E). CSRP2 knockdown did not reduce the protein levels of β-catenin or its targets, MYC and CYCLIN D1 (Figure 6F; Figure S4B). Conversely, treatment with siRNA against β-catenin also inhibited DT cell proliferation, but had no effect on CSRP2 levels. Regarding possible crosstalk between β-catenin signaling and TGF-β signaling, β-catenin knockdown did not affect the phosphorylation level of Smad2 or mRNA levels of *Tgfb1*, *-2*, and *-3* in DT cells (Figure S4C,D). Treatment with SB431542, a TGF-β pathway inhibitor, had no effect on β-catenin levels (Figure 6B). In addition, suppression of cell proliferation by knockdown of β-catenin siRNA was enhanced in the presence of SB431542 (Figure S4E). These findings suggested that TGF-β signaling fosters the growth of DT cells independently of β-catenin. Importantly, CSRP2 overexpression significantly reduced the growth suppressive effect of SB431542 (Figure S4F,G). CSRP2 knockdown in DT cells did not reduce the mRNA levels of *Col1a1* or *Tgfb1*, *-2*, and *-3*; however, it significantly decreased those of *Col5a* and *Vim* (vimentin) (Figure S4H). Thus, increased CSRP2 expression through activation of the TGF-β pathway in DT cells may contribute to the growth and spread of DTs through the induction of these genes. Taken together, our results indicated that CSRP2 was involved in the proliferation of DT cells downstream of the TGF-β/SMAD4 signaling pathway.

4 | DISCUSSION

In this study, we demonstrated that the local induction of a β-catenin mutation in PDGFRA-expressing stromal cells by subcutaneous injection of 4HT led to the formation of DTs with 100% penetrance. Proliferation of uniform spindle cells, resembling myofibroblasts with abundant collagenous stroma, positive staining for β-catenin, vimentin, CD44, desmin, Sca1, and Thy1, and negative staining for CD31, authenticated this mouse model of extra-abdominal DTs. Previous mouse models of DTs include Apc1638N mice with a heterozygous mutation in the *Apc* gene and *Ng2/Scpg4-CreER;Ctnnb1*^{ex3} mice.[22,23]

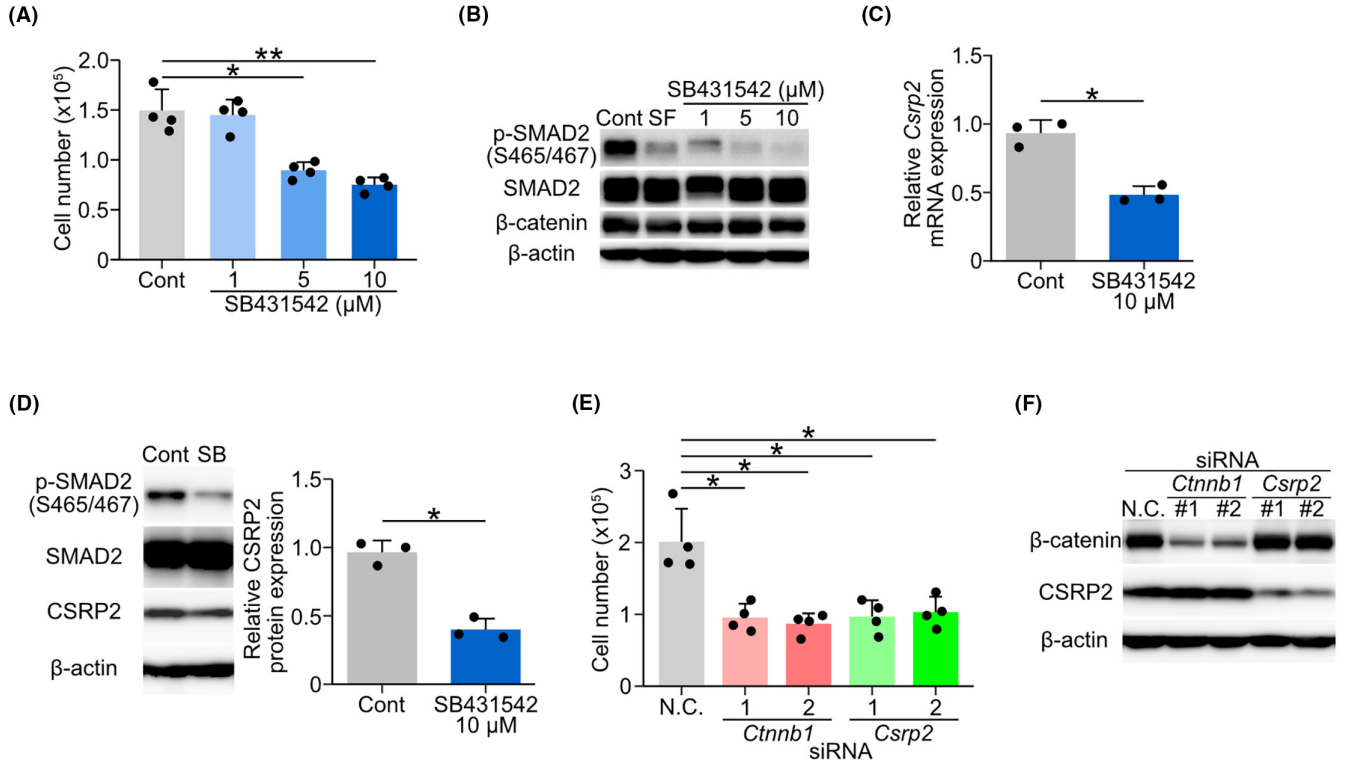

FIGURE 6 CSRP2 is positively regulated by TGF-β/SMAD4 signaling and is involved in the proliferation of desmoid tumor cells. (A) Proliferation of desmoid tumors from *Pdgfra-Cre*ERT2;*Ctnnb1*$^{+/flox(ex3)}$/*Trp53*$^{+/flox}$ mouse. Cells were counted 72 h after seeding 1×10^4 cells. Cells were treated with SB431542 24 h after plating and then cultured for 48 h. Data are presented as dot and bar plots. Data are given as means ± SD ($n=4$), and assessed using one-way ANOVA and Tukey's HSD test. *$p<0.001$, **$p<0.0001$. Cont: control (DMSO treatment). (B) Western blots of phospho-SMAD2 (p-SMAD2) and β-catenin in desmoid tumor cells treated with SB431542 or vehicle only in the presence of serum for 48 h. Cont: control (DMSO treatment). SF, cultured in serum-free condition for 24 h. (C) RT-qPCR analysis of CSRP2 expression in desmoid tumor cells treated with SB431542 or vehicle only for 48 h. Data are presented as dot and bar plots. Data are given as means ± SD ($n=3$), and assessed using a two-tailed Student's *t*-test. *$p<0.01$. Cont: control (DMSO treatment). (D) Effect of SB431542 on CSRP2 protein expression in DT cells. (Left) Western blots of CSRP2 in desmoid tumor cells treated with 10 μM SB431542 or vehicle only for 48 h (SB). (Right) Quantification of the left panel. Band intensity of CSRP2 was quantified using ImageJ software and normalized against β-actin. Data are given as means ± SD ($n=3$), and assessed using a two-tailed Student's *t*-test. *$p<0.05$. Cont, control (DMSO treatment). (E) Effect of siRNA against *Csrp2* or *Ctnnb1*(β-catenin) on the proliferation of desmoid tumor cells. Cells were counted 72 h after seeding 2×10^4 cells. Cells were treated with siRNAs 24 h after plating and then cultured for 48 h. N.C., negative control siRNA. Data are presented as dot and bar plots. Data are given as means ± SD ($n=4$), and assessed using one-way ANOVA and Tukey's HSD test. *$p<0.005$. (F) Western blots of CSRP2 and β-catenin in desmoid tumor cells treated with siRNAs as in (E).

The former model developed DTs at several locations in association with striated muscle via LOH at the *Apc* locus, whereas DTs in the latter model were induced by intraperitoneal injection of 4HT, leading to the expression of stable β-catenin in pericytes. Our model is unique in that DTs can be locally induced by subcutaneous injection of 4HT. Desmoid tumors induced by tamoxifen in this model were larger in the backs of mice than in the femurs (Figure S1A). This disparity could be attributed to the greater area in the backs of mice, which may contain larger populations of PDGRFA-positive cells under the skin. We consider fibroblasts or mesenchymal stem cells as the cells that originate DTs in our model. However, PDGFRα is reportedly expressed in a subpopulation of pericytes[24]; thus, a possible pericyte origin cannot be completely excluded. Tracking of DT growth in C mice using IVIS revealed that tumors tended to stabilize and sometimes regressed temporarily over time. This observation was not expected but may reflect clinical situations because DTs in patients sometimes show stabilization of growth and spontaneous regression.[25]

We found that SMAD4 knockout significantly suppressed DT formation accompanying reduced proliferation of tumor cells, providing genetic evidence for TGF-β/SMAD4 signaling in DT growth (Figure 3A–C). Consistent with this finding in vivo, treatment with the TGF-β receptor inhibitor, SB431542, strongly attenuated proliferation of DT cells in vitro (Figure 6A). A previous report showed that TGF-β signaling positively regulates the proliferation of patient-derived DT cells in vitro in a SMAD-dependent manner using SIS3, a SMAD3 inhibitor.[20] A more recent study demonstrated therapeutic implications for dependence on the TGF-β pathway of DTs and showed the effectiveness of TGF-β receptor inhibitors in suppressing the growth of patient-derived DT cells.[26] Our proteomic and in vitro analyses using DT cells revealed that CSRP2 is a key molecule in their proliferation downstream of TGF-β/SMAD4 signaling

(Figures 5A–D and 6C,D). Expression of CSRP2 was confirmed in clinical samples from DT patients (Figure 5E; Figure S3). Microarray analysis indicated that CSRP2 is differentially expressed in tumors and normal fascia from DT patients, and is upregulated in DTs in 75% of patients.[27]

CSRP2 protein is a member of the CSRP family, characterized by the presence of two LIM zinc-binding domains, and is predominantly localized in the cytoplasm and nucleus. CSRP2 significantly influences the regulation of motility, differentiation, and the growth of smooth muscle cells and fibroblasts by interacting with cytoskeleton proteins, including F-actin, as well as with transcription factors such as serum response factor (SRF), GATA, and myocardin-related transcription factors (MRTF).[28–31] TGF-β upregulates CSRP2 in VSMCs at the transcriptional level through ATF2, thereby enhancing their motility.[32] In vascular hypertension, TGF-β-driven expression of CSRP2 in vascular fibroblasts contributes to vascular fibrosis by promoting nuclear translocation of YAP/TAZ. Additionally, in myofibroblasts and cancer-associated fibroblasts (CAF), TGF-β-induced CSRP2 associates with MRTFs, consequently promoting the collective invasion of cancer cells.[31,33] These findings imply that elevated expression of CSRP2, triggered by activation of the TGF-β pathway in DT cells, may stimulate growth and expansion of DTs through mechanisms described above (Figure 6). Identifying the partners of CSRP2 that are essential for its functions in DTs will be a pivotal area of emphasis in our future research.

In conclusion, we propose this model of subcutaneous 4-hydroxy-tamoxifen injection into *Pdgfra-Cre*^{ERT2};*Ctnnb1*$^{flox(ex3)}$ mice as a new mouse model of sporadic, extra-abdominal DTs, which can be used to study mechanisms of their pathogenesis and for pre-clinical studies of novel therapies. Our study also indicates that the TGF-β/CSRP2 axis is a potential biomarker and/or therapeutic target for DTs.

AUTHOR CONTRIBUTIONS

Yu Li: Investigation; writing – original draft. **Teruaki Fujishita:** Conceptualization; data curation; formal analysis; funding acquisition; investigation; project administration; supervision; visualization; writing – original draft; writing – review and editing. **Emi Mishiro-Sato:** Data curation; investigation. **Yasushi Kojima:** Data curation; formal analysis. **Yanqing Niu:** Investigation. **Makoto Mark Taketo:** Resources. **Yuya Urano:** Investigation. **Tomohisa Sakai:** Resources. **Atsushi Enomoto:** Investigation. **Yoshihiro Nishida:** Conceptualization; resources. **Masahiro Aoki:** Conceptualization; funding acquisition; investigation; project administration; supervision; writing – review and editing.

ACKNOWLEDGMENTS

We thank Kyoko Kobori, Yoshiko Goto, and Akiko Kato for technical assistance, and Kentaro Taki (Division for Medical Research Engineering, Nagoya University Graduate School of Medicine) for technical support of LC–MS. This work was supported by JSPS KAKENHI Grant Numbers JP20K07440 (to TF), JP17H01585 (to YN), and JP18H02686 (to MA).

CONFLICT OF INTEREST STATEMENT

The authors declare no competing financial interests in relation to the work described.

Masahiro Aoki, Atsushi Enomoto, and Yoshihiro Nishida are Editorial Board members of *Cancer Science*.

DATA AVAILABILITY STATEMENT

RNA sequence data are available from the DNA Data Bank of Japan (DDBJ): Sequenced Read Archive under accession number DRA016294.

ETHICS STATEMENT

Approval of the research protocol by an Institutional Reviewer Board: This study was approved by the Ethics Committee of Nagoya University Graduate School of Medicine (approval numbers 2014-0280-4 and 2017-0127-5).

Informed Consent: Informed consent was obtained in the form of the opt-out on the website.

Registry and the Registration No. of the study/trial: N/A.

Animal Studies: All animal experiments were carried out according to protocols approved by the Animal Care and Use Committee of Aichi Cancer Center Research Institute.

ORCID

Teruaki Fujishita https://orcid.org/0000-0002-4397-2438
Yasushi Kojima https://orcid.org/0000-0002-0087-1768
Atsushi Enomoto https://orcid.org/0000-0002-9206-6116
Yoshihiro Nishida https://orcid.org/0000-0002-7511-6388
Masahiro Aoki https://orcid.org/0000-0003-4316-9490

REFERENCES

1. Kasper B, Raut CP, Gronchi A. Desmoid tumors: to treat or not to treat, that is the question. *Cancer*. 2020;126:5213-5221.
2. Garcia-Ortega DY, Martín-Tellez KS, Cuellar-Hubbe M, et al. Desmoid-type fibromatosis. *Cancers*. 2020;12:1851.
3. Salas S, Chibon F, Noguchi T, et al. Molecular characterization by array comparative genomic hybridization and DNA sequencing of 194 desmoid tumors. *Genes Chromosomes Cancer*. 2010;49:560-568.
4. Trautmann M, Rehkämper J, Gevensleben H, et al. Novel pathogenic alterations in pediatric and adult desmoid-type fibromatosis – a systematic analysis of 204 cases. *Sci Rep*. 2020;10:3368.
5. Kohsaka S, Hirata M, Ikegami M, et al. Comprehensive molecular and clinicopathological profiling of desmoid tumours. *Eur J Cancer*. 2021;145:109-120.
6. Desmoid Tumor Working Group. The management of desmoid tumours: a joint global consensus-based guideline approach for adult and paediatric patients. *Eur J Cancer*. 2020;127:96-107.
7. Kahn M. Can we safely target the WNT pathway? *Nat Rev Drug Discov*. 2014;13:513-532.
8. Harada N, Tamai Y, Ishikawa T, et al. Intestinal polyposis in mice with a dominant stable mutation of the beta-catenin gene. *EMBO J*. 1999;18:5931-5942.
9. Prieto C, Barrios D. RaNA-Seq: interactive RNA-Seq analysis from FASTQ files to functional analysis. *Bioinformatics*. 2020;36:1955-1956.
10. Fujishita T, Kojima Y, Kajino-Sakamoto R, et al. The cAMP/PKA/CREB and TGFβ/SMAD4 pathways regulate stemness

and metastatic potential in colorectal cancer cells. *Cancer Res*. 2022;82:4179-4190.
11. Zhou Y, Zhou B, Pache L, et al. Metascape provides a biologist-oriented resource for the analysis of systems-level datasets. *Nat Commun*. 2019;10:1523.
12. Livak KJ, Schmittgen TD. Analysis of relative gene expression data using real-time quantitative PCR and the 2(-Delta Delta C(T)) method. *Methods*. 2001;25:402-408.
13. Fujishita T, Kojima Y, Kajino-Sakamoto R, Taketo MM, Aoki M. Tumor microenvironment confers mTOR inhibitor resistance in invasive intestinal adenocarcinoma. *Oncogene*. 2017;36:6480-6489.
14. Liegl B, Leithner A, Bauernhofer T, et al. Immunohistochemical and mutational analysis of PDGF and PDGFR in desmoid tumours: is there a role for tyrosine kinase inhibitors in c-kit-negative desmoid tumours? *Histopathology*. 2006;49:576-581.
15. Miwa H, Era T. Generation and characterization of PDGFRα-GFPCreERT2 knock-in mouse line. *Genesis*. 2015;53:329-336.
16. Bolontrade M, García M. *Mesenchymal Stromal Cells as Tumor Stromal Modulators*. Academic Press; 2016:642.
17. Ferenc T, Sygut J, Kopczyński J, et al. Aggressive fibromatosis (desmoid tumors): definition, occurrence, pathology, diagnostic problems, clinical behavior, genetic background. *Pol J Pathol*. 2006;57:5-15.
18. Budi EH, Schaub JR, Decaris M, Turner S, Derynck R. TGF-β as a driver of fibrosis: physiological roles and therapeutic opportunities. *J Pathol*. 2021;254:358-373.
19. Braun AC, Campos FAB, Abdallah EA, et al. Circulating tumor cells in desmoid tumors: new perspectives. *Front Oncologia*. 2021;11:622626.
20. Enzo MV, Cattelan P, Rastrelli M, et al. Growth rate and myofibroblast differentiation of desmoid fibroblast-like cells are modulated by TGF-β signaling. *Histochem Cell Biol*. 2019;151:145-160.
21. Wei J, Gorman TE, Liu X, et al. Increased neointima formation in cysteine-rich protein 2-deficient mice in response to vascular injury. *Circ Res*. 2005;97:1323-1331.
22. Smits R, van der Houven van Oordt W, Luz A, et al. Apc1638N: a mouse model for familial adenomatous polyposis-associated desmoid tumors and cutaneous cysts. *Gastroenterology*. 1998;114:275-283.
23. Sato S, Tang YJ, Wei Q, et al. Mesenchymal tumors can derive from Ng2/Cspg4-expressing pericytes with β-catenin modulating the neoplastic phenotype. *Cell Rep*. 2016;16:917-927.
24. Hung C, Linn G, Chow Y-H, et al. Role of lung pericytes and resident fibroblasts in the pathogenesis of pulmonary fibrosis. *Am J Respir Crit Care Med*. 2013;188:820-830.
25. Kasper B, Ströbel P, Hohenberger P. Desmoid tumors: clinical features and treatment options for advanced disease. *Oncologist*. 2011;16:682-693.
26. Yun K-H, Park C, Ryu HJ, et al. Therapeutic implications of TGF-β pathway in desmoid tumor based on comprehensive molecular profiling and clinicopathological properties. *Cancer*. 2022;14:5975.
27. Denys H, Jadidizadeh A, Amini Nik S, et al. Identification of IGFBP-6 as a significantly downregulated gene by beta-catenin in desmoid tumors. *Oncogene*. 2004;23:654-664.
28. Weiskirchen R, Pino JD, Macalma T, Bister K, Beckerle MC. The cysteine-rich protein family of highly related LIM domain proteins. *J Biol Chem*. 1995;270:28946-28954.
29. Grubinger M, Gimona M. CRP2 Is an autonomous Actin-binding protein. *FEBS Lett*. 2004;557:88-92.
30. Chang DF, Belaguli NS, Iyer D, et al. Cysteine-rich LIM-only proteins CRP1 and CRP2 are potent smooth muscle differentiation cofactors. *Dev Cell*. 2003;4:107-118.
31. Hayashi K, Horoiwa S, Mori K, et al. Role of CRP2-MRTF interaction in functions of myofibroblasts. *Cell Struct Funct*. 2023;48:83-98.
32. Lin D-W, Chang I-C, Tseng A, et al. Transforming growth factor beta up-regulates cysteine-rich protein 2 in vascular smooth muscle cells via activating transcription factor 2. *J Biol Chem*. 2008;283:15003-15014.
33. Chen X, Wei X, Ma S, et al. Cysteine and glycine rich protein 2 exacerbates vascular fibrosis in pulmonary hypertension through the nuclear translocation of yes-associated protein and transcriptional coactivator with PDZ-binding motif. *Toxicol Appl Pharmacol*. 2022;457:116319.

SUPPORTING INFORMATION

Additional supporting information can be found online in the Supporting Information section at the end of this article.

How to cite this article: Li Y, Fujishita T, Mishiro-Sato E, et al. TGF-β signaling promotes desmoid tumor formation via CSRP2 upregulation. *Cancer Sci*. 2024;115:401-411. doi:10.1111/cas.16037